Frequency-resonance-enhanced vibrational resonance in bistable systems

Chenggui Yao,[1,2] Yan Liu,[1,2] and Meng Zhan[1,*]
[1]*Wuhan Institute of Physics and Mathematics, Chinese Academy of Sciences, Wuhan 430071, China*
[2]*Graduate School of the Chinese Academy of Sciences, Beijing 100049, China*
(Received 30 March 2011; revised manuscript received 14 May 2011; published 16 June 2011)

The dynamics in an overdamped bistable system subject to the action of two periodic forces (assuming their frequencies are ω and Ω, and amplitudes are A and B, respectively) is studied. For the usual vibrational resonance, the nonmonotonic dependence of signal output of the low frequency ω on the change of B for a fixed Ω, the condition $\Omega \gg \omega$ is always assumed in all previous studies. Here, removing this restriction, we find that a resonant behavior can extensively occur with respect to the changes of both the frequency Ω and amplitude B. Especially, the resonance becomes stronger when Ω is chosen such that it is exactly in frequency resonance with ω. This combinative behavior, called *frequency-resonance-enhanced vibrational resonance*, is of great interest and may shed an improved light on our understanding of the dynamics of nonlinear systems subject to a biharmonic force.

DOI: 10.1103/PhysRevE.83.061122 PACS number(s): 05.40.Ca, 87.16.dj

I. INTRODUCTION

Stochastic resonance, the phenomenon of the response of nonlinear systems to a weak periodic signal enhanced by an appropriate amount of noise, has drawn much attention in nonlinear sciences for more than 30 years [1–3]. The constructive role of noise has been extensively studied in a variety of nonlinear systems, e.g., bistable systems [4,5], monostable systems [6], excitable systems [7], nondynamical threshold models [8], and ensembles of interacting nonlinear elements [9]. Considerable works on theoretic analysis [10] and experimental observations [11] have been conducted, and now the focus has been moved to its applications in diverse fields.

Recently, a high-frequency signal, as another type of excitation, has been proposed in the context of stochastic resonance and found that it can play a similar role as noise [12–15]. The system's response to a weak low-frequency signal can also become maximal by an appropriate choice of vibration amplitude for the high-frequency signal. This phenomenon is referred to as vibrational resonance. Since biharmonic signals are pervasive in many science and application fields, such as acoustics [16], neuroscience [17], laser physics [18], engineering [19], and even the Global Positioning System [20], the study of vibrational resonance is of great significance, and indeed it has been widely investigated in various systems, including excitable [21–24], bistable [25–28], and spatially extended systems, etc. [29–31]. Chizhevsky *et al*. provided the first experimental evidence of vibrational resonance in a bistable vertical cavity laser system [32]. A recent theoretical study demonstrated that with the change of driving amplitude, a high-frequency signal may induce a system transition from bistable to monostable and result in a substantial change of the system response across the critical point [33].

Although vibrational resonance is called resonance, it has little in common with the classical concept of (frequency) resonance [34]. Vibrational resonance means the resonant amplification of the signal output with respect to the *amplitude* of the external force, which is usually assumed as high frequency, whereas frequency resonance means its resonant amplification with respect to the *frequency* of the external force, especially when it becomes exactly equal to or is multiples of the natural frequency of the system. Therefore, basically, vibrational resonance is an amplitude effect and frequency resonance is a frequency effect. In frequency resonance, small periodic driving forces can produce a large amplitude output, whereas in vibrational resonance, only sufficiently large periodic driving forces can produce a large amplitude effect. So far, to the best of our knowledge, in all existing works on vibrational resonance, the condition for a biharmonic force with two very different frequencies was always preassumed, and thus the possible connection and interplay between vibrational resonance and frequency resonance remains unclear.

In this paper, we attempt to study vibrational resonance within the whole parameter plane constructed by the parameters of amplitude and frequency, in the absence of the condition of two frequencies being very different. We find that vibrational resonance can appear under the condition of only two low frequencies, and more interestingly, the frequency-resonance effect may even be superimposed on the vibrational resonance curve. These findings show the combinative effects of the system nonlinearity and two external competitive signals.

II. MODEL

We still consider the classical model written by

$$\dot{x} = x - x^3 + A\cos(\omega t) + B\cos(\Omega t + \phi). \qquad (1)$$

The model describes the overdamped motion in the bistable potential $U(x) = \frac{x^4}{4} - \frac{x^2}{2}$ subject to the modulation of two different periodic signals with frequencies ω ($\omega = 2\pi/T$) and Ω ($\Omega = 2\pi/T'$), respectively. Their corresponding driving intensities (amplitudes) are A and B. Different with previous studies on vibrational resonance with the restriction of $\Omega \gg \omega$, here we are interested in the system response with Ω capable of being freely chosen. Namely, the value of Ω can be tuned from zero to a very large number. Without losing generality, the first periodic signal is always set to be weak (subthreshold)

*zhanmeng@wipm.ac.cn

and of low frequency ($A \ll 1$ and $\omega \ll 1$). Therefore, without the second signal Ω, no system transition can occur. Under this condition, B is always sufficiently larger than A and the term $A\cos(\omega t)$ in Eq. (1) can be ignored, and thus the value of ϕ is not important. However, if the values of B and A are comparable ($A \ll 1$ and $B \ll 1$), ϕ should be important in the resonance case $\Omega = n\omega$; a similar idea has been applied in the chaos control within the framework of the phase control method [35]. In this paper, the parameters $A = 0.1, \omega = 0.2$, and $\phi = 0$ are always chosen and fixed. For the computer simulation of Eq. (1), the standard fourth-order Runge-Kutta approach with a fixed time step $\Delta t = 0.01$ is applied.

To quantify the response of the system to the first weak periodic signal, we calculate Q [12],

$$Q = \sqrt{Q_c^2 + Q_s^2}/A,$$

$$Q_c = \frac{2}{nT}\int_0^{nT} x(t)\cos(\omega t)dt, \tag{2}$$

$$Q_s = \frac{2}{nT}\int_0^{nT} x(t)\sin(\omega t)dt,$$

after discarding transient processing. Clearly the value of Q is proportional to the Fourier transform coefficient $F(\omega')$ at $\omega' = \omega$ [$F(\omega') = \int_0^{+\infty} e^{i\omega' t}x(t)dt$], i.e.,

$$Q \propto |F(\omega' = \omega)|. \tag{3}$$

The benefit of calculating Q is that it is direct and fast, as we do not need to calculate the Fourier transform spectrum for all ω'.

III. OBSERVATIONS AND RESULTS

Figures 1(a) and 1(b) show Q as a function of Ω and B in a three-dimensional (3D) plot and a two-dimensional (2D) contour plot, respectively. Clearly the usual vibrational resonance occurs with a change in B for a sufficiently large, fixed Ω ($\Omega \gg \omega$). Say, e.g., $\Omega = 5.0$. These resonance peaks can also be viewed to exist in the Ω direction for a fixed B, and their height is nearly unchanged for $\Omega \gg \omega$ and $B \gg 1$. With a decrease of both Ω and B, surprisingly, we find that the value of Q may even become larger, compared to the constant value within the high-frequency Ω region. Roughly, the peak is located at $\Omega \approx 0.7$. With a further decrease of Ω and B, along the peak curve Q quickly damps and vanishes. As a result, a clear resonant curve for the local maximum Q appears on the (Ω, B) plane and its peak value depends on the values of both Ω and B. Explicitly, we may denote its locus as (Ω^*, B^*).

If we take a closer look at the pattern in Fig. 1, we can well recognize some small, sharp resonant peaks on the resonant curve, which clearly come from frequency resonance between ω and Ω. We show Q vs Ω^* in Fig. 2(a) and its magnified plot in Fig. 2(b). Clearly these peaks are located at $\Omega = n\omega$, for $n = 2$, 3, and 4. Based on these observations, we may call it *frequency-resonance-enhanced vibrational resonance*. It is notable that these sharp resonant peaks are located above the

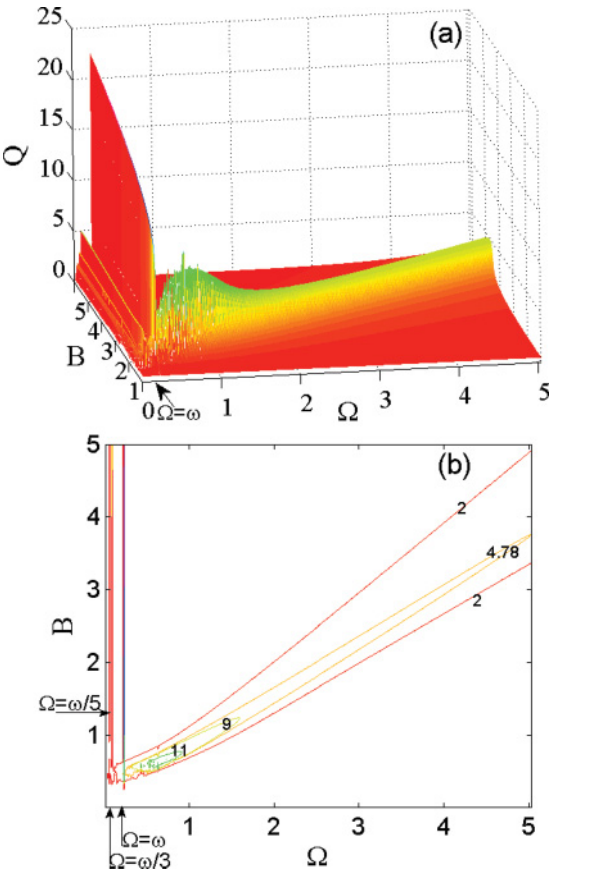

FIG. 1. (Color online) (a) and (b) The 3D plot and contour plot of response Q as a function of Ω and B. The other parameters, $A = 0.1$, $\omega = 0.2$, and $\phi = 0$, are fixed.

vibrational resonance curve and depend on the values of both Ω^* and B^*.

All these findings indicate that the vibrational resonance, which has long been believed to occur only with two very different frequencies (one is low-frequency and the other is high-frequency), actually can appear in a much broader parameter region. More interestingly, the system response gets stronger at proper values of both Ω and B (usually Ω is only several times of ω); this gives rise to the vibrational resonance at small Ω and the frequency-resonance-enhanced vibrational resonance at $\Omega = n\omega$.

In Fig. 1, for even smaller Ω, something unusual appears. Q monotonically increases with B, when $\Omega = \omega$ is chosen. This is easy to understand. For several other discrete values of Ω ($\Omega < \omega$), it appears that the monotonic increase of Q vs B is unchanged. At the end of the paper, we will give a detailed discussion on this phenomenon.

In Ref. [33], the vibrational resonance of a high-frequency force was theoretically studied by the method of inertial approximation, with which, relying on $\Omega \gg \omega$, $x(t)$ in Eq. (1) can be decomposed into a slow motion $X(t)$ and a fast motion $\Psi(t)$, and the evolution equation of the slow motion $X(t)$ can be written as

$$\dot{X} = \left(1 - \frac{3B^2}{2\Omega^2}\right)X - X^3 + A\cos(\omega t). \tag{4}$$

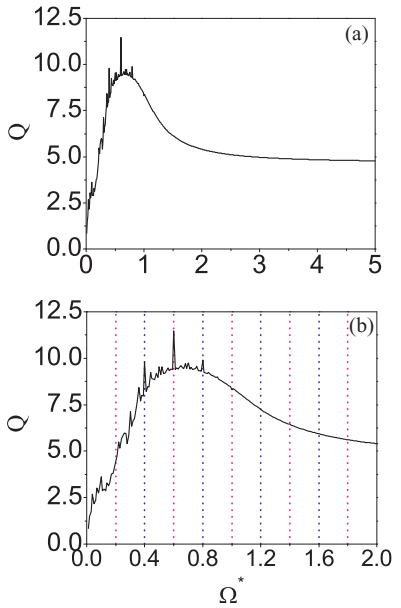

FIG. 2. (Color online) (a) Q vs Ω^* and (b) its magnification plot, showing the resonant curve of Q vs Ω^* (also B^*) on the locus of the bifurcation parameter (Ω^*, B^*) and the frequency-resonance-enhanced vibrational resonance effect. $\omega = 0.2$.

Based on the bifurcation analysis of such a simplified equation and the dynamical stabilization of the unstable point, quantitatively we have [33]

$$Q = \begin{cases} \dfrac{1}{\sqrt{\omega^2 + 4\left(1 - \frac{3B^2}{2\Omega^2}\right)^2}}, & \mathrm{B} < \mathrm{B_{c1}}, \\ \dfrac{1}{\sqrt{\omega^2 + \left(1 - \frac{3B^2}{2\Omega^2}\right)^2}}, & \mathrm{B} \geqslant \mathrm{B_{c1}}, \end{cases} \tag{5}$$

where

$$B_{c1} = \Omega\sqrt{\frac{2}{3}}. \tag{6}$$

Clearly Q increases with B at $B < B_{c1}$ and decreases with B at $B \geqslant B_{c1}$, and a vibrational resonance curve of Q vs B appears. Due to this linear dependence of B_{c1} on Ω, a vibrational resonance with Ω also exists, which is exactly what we see in Fig. 1 for $\Omega \gg \omega$ and $B \gg 1$. Thus the high-frequency signal can change the dynamics of the slow motion, giving rise to a system transition from bistable to monostable, and make the amplitude of the slow motion become maximal at the transition point. Therefore, theoretically the peak position for the vibrational resonance should correspond to the system threshold from bistable to monostable.

Our numerical result shows that this is correct and the above picture can be generalized to the whole Ω parameter region. In Fig. 3, the local maximum data in Fig. 1 indicating (Ω^*, B^*) are chosen and plotted by a solid line, and the threshold data from bistable to monostable denoted by B_c are numerically obtained and plotted by a dashed line. [As some examples, bifurcation diagrams of $x(t)$ for different Ω's are illustrated in Fig. 4, where the dynamical changes across point B_c are clear.] Comparing these two lines, we find that they match mostly, except for a slight deviation for large Ω. This mismatch can

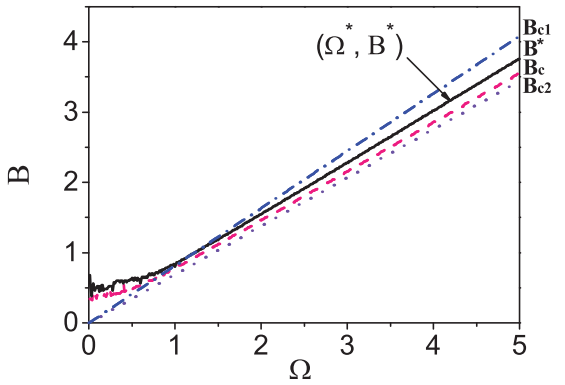

FIG. 3. (Color online) The plots of B^* (solid line), B_c (dashed line), B_{c1} (dashed-dotted line) from Eq. (6), and B_{c2} (dotted line) from Eq. (7) vs Ω. Obviously, for any Ω, the peak of the vibrational resonance at (Ω^*, B^*) originates from the system bifurcation from bistable to monostable at B_c.

also be found in the experimental and numerical observations in Ref. [33]. Therefore, we know that basically within the whole (Ω, B) parameter plane, the vibrational resonance exists and comes from the system transition from bistable to monostable, with the feature independent of the specific value of Ω.

For comparison, the theoretical prediction B_{c1} in Eq. (6) is shown with a dashed-dotted line in Fig. 3. In addition, another prediction B_{c2},

$$B_{c2} = \Omega\sqrt{\frac{2(1-u^*)}{3}}, \tag{7}$$

$$u^* = S_+ + S_-, \quad S_\pm = \left[3A^2 \pm \left[9A^4 + \frac{6\omega^6}{27}\right]^{1/2}\right]^{1/3},$$

according to the method of harmonic balance [36], is also calculated and plotted by a dotted line. Obviously, it fits the line B_c well, but it still deviates the line B^*.

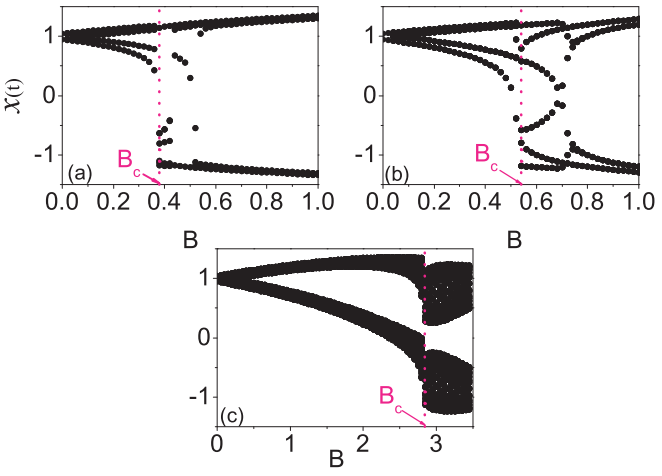

FIG. 4. (Color online) (a)–(c) Bifurcation diagrams of $x(t)$ for different values of Ω: $\Omega = 0.12$, 0.6, and 4.0, respectively, indicating the system transition from bistable to monostable across the threshold B_c.

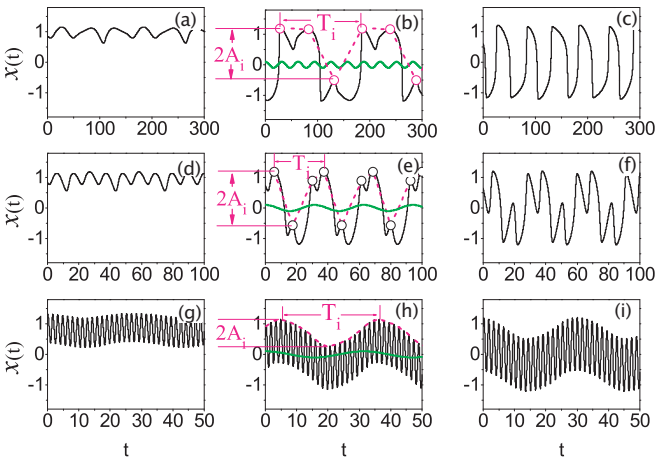

FIG. 5. (Color online) Time series $x(t)$ for different parameter values of Ω and B. From the top row to the bottom row, different Ω's are chosen: $\Omega = 0.12$, 0.6, and 4.0, respectively. From the left-hand column to the right-hand column, different B's are chosen: $B < B^*, B = B^*$, and $B > B^*$, respectively. Specifically, $B = 0.3$ (a), 0.44 (b), 0.5 (c), 0.4 (d), 0.56 (e), 0.7 (f), 2.0 (g), 2.8 (h), and 3.5 (i). In the middle column, how to calculate period T_i and amplitude A_i of the slow motion is schematically shown, and the solid lines stand for the periodic signal $A\cos(\omega t)$.

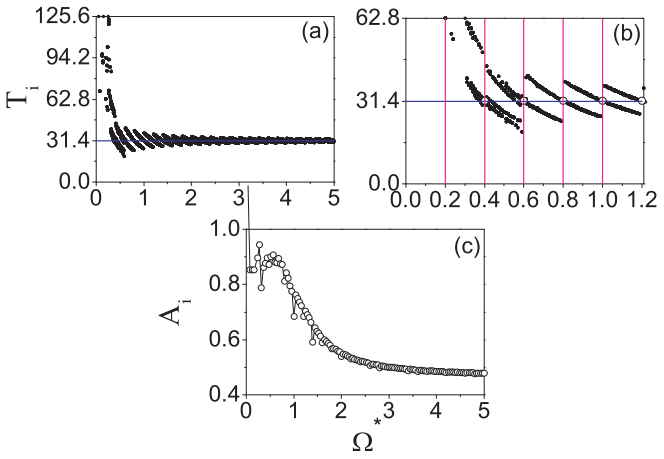

FIG. 6. (Color online) (a) and (c) T_i and A_i (from Fig. 5) vs Ω^*. (b) The zoomed-in picture of (a), showing $T_i = T \approx 31.4$ at $\Omega^* = n\omega$. Clearly the resonant curve in Fig. 2 comes from the coaction of T_i and A_i.

In order to make the dynamical behaviors clearer, the time series of $x(t)$ in Eq. (1) for different parameter values of Ω and B are given in Fig. 5. For the rows, from top to bottom, $\Omega = 0.12$, 0.6, and 4.0. For the columns, from left to right, different values of B ($B < B^*, B = B^*$, and $B > B^*$) are chosen. Comparing any three subfigures in each row, we do find the dynamical change from bistable to monostable. For different Ω's, we also find a stronger high-frequency modulation effect with an increase of Ω (comparing the third row with the first two rows).

So far we know that the vibrational resonance can occur for all Ω's as shown in Fig. 1. However, the problem as to why the resonance occurs on the bifurcation parameter curve (Ω^*,B^*) as shown in Fig. 2 remains unanswered. We do not understand why for proper intermediate values of Ω and B the system can oppositely respond stronger, as compared to much larger values of Ω and B. We also do not understand how the frequency-resonance-enhanced vibrational resonance occurs. To this end, we study the time series $x(t)$ on the parameter set (Ω^*,B^*), as shown the middle column in Fig. 5, and check their changes. For example, we first select all the local maximum points (denoted by open circles), and then calculate the system instantaneous period T_i by the time interval between any two successive maximum points among all these selected points and the system amplitude $2A_i$ by the amplitude difference between any two successive maximum and minimum points among all these selected points again. The calculation process is schematically shown in the figures. The values of T_i and A_i should catch the essential feature of the system dynamics, the slow motion. The results for T_i and A_i with a change of Ω^* are shown in Figs. 6(a) and 6(c). The magnification of Fig. 6(a) is shown in Fig. 6(b). From these figures, we can find that T_i is multivalued, except for several discrete parameters at $\Omega^* = n\omega$ and $n \geqslant 2$, which is much clearer in Fig. 6(b). Only at these parameters (open circles) is T_i exactly equal to the low-frequency period T, i.e., $T_i = T = 2\pi/\omega \approx 31.4$. Meanwhile, in Fig. 6(c), with an increase of Ω^*, A_i monotonically decreases from $A_i \approx 0.9$ to 0.5, after the first approximately constant region ($\Omega^* \leqslant 0.8$). Based on these observations, Q monotonically increases with Ω for small Ω, as T_i becomes ordered and saturates to T, and meanwhile A_i is independent of the change of Ω. After that ($\Omega \approx 0.7$), Q monotonically decreases with Ω due to the monotonic decrease of A_i. Hence the nonmonotonic resonancelike dependence of Q on Ω^* (also B^*) occurs in Fig. 2. On the other hand, the values of Q become much larger at the resonant frequencies: $\Omega = n\omega$ and the resonant effect becomes enhanced, due to exact match of T_i with T. When $\Omega \gg \omega$, the frequency resonant effect fades. Since the system response should be contributed to by both the amplitude and phase of the slow motion, now it is easy to understand the occurrences of the resonant curve with Ω^* and the frequency-resonance-enhanced effect in Fig. 2.

Finally, let us move to the smaller Ω parameter region ($\Omega < \omega$) and study the underlying mechanism for the peaks. A detailed study shows that these peaks only occur at some specific values of Ω: $\Omega = \frac{\omega}{n}$, where n is odd. In Fig. 7(a), Q is plotted as a function of B for $\Omega = \frac{\omega}{3}, \frac{\omega}{5}, \frac{\omega}{7}, \frac{\omega}{9}$; clearly Q monotonically increases after the first fluctuation region for small B. In Fig. 7(b), Q is plotted as a function of Ω for a fixed $B = 5.0$; the peaks at $\Omega = \omega, \frac{\omega}{3}, \frac{\omega}{5}, \ldots$, are clear. In Figs. 7(c) and 7(d), the time series $x(t)$ and the corresponding power spectra are shown, respectively, for $\Omega = 0.03$ (solid line) and $\Omega = 0.04 = \frac{\omega}{5}$ (dotted line); $B = 5.0$. Clearly as now a sufficiently large B is generally considered ($B \gg A$) and $\Omega < \omega$, the system will perform a periodic motion with the period T' ($T' = 2\pi/\Omega$). This is a key difference with the situation of $\Omega > \omega$. Based on the symmetric potential in Eq. (1), we have the system must be invariant under the parity symmetry transformation $\mathcal{T}: x \to -x, t \to t + \frac{T'}{2}$, i.e., $x(t + \frac{T'}{2}) = -x(t)$, and further $x(t)$ should possess only odd Fourier coefficients [2]. This point has been well confirmed by Fig. 7(d), where only odd Fourier spectrum peaks at $\omega' = \Omega$,

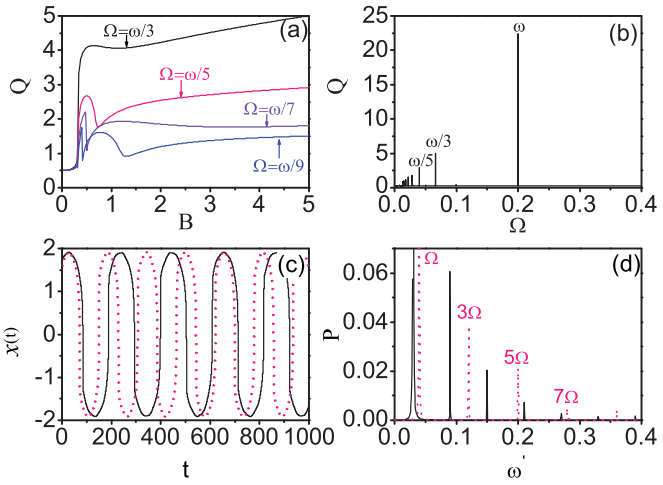

FIG. 7. (Color online) The study of signal enhancement at $\Omega < \omega$. (a) Q vs B for $\Omega = \frac{\omega}{3}, \frac{\omega}{5}, \frac{\omega}{7}, \frac{\omega}{9}$. (b) Q vs Ω for a fixed B ($B = 5.0$). (c) and (d) The time series $x(t)$ and its power spectra, respectively, for $\Omega = 0.03$ (solid line) and 0.04 (dotted line); $B = 5.0$ and $\omega = 0.2$. For $\Omega = \omega/5 = 0.04$, a peak appears at $\omega' = \omega = 5\Omega$ in the spectrum in (d), giving rise to the peak at $\Omega = \omega/5 = 0.04$ in the pattern of Fig. 1.

3Ω, 5Ω, and 7Ω exist. Therefore, it is easy to understand the observations in Figs. 1 and 7(b) for the peaks existing only at some specific values of Ω: $\Omega = \omega/n$, with n being odd. As a result, for $\Omega < \omega$ these peaks might simply come from the coincidence of the two frequencies ω and Ω (or their components); they are fundamentally different with the resonant effect for $\Omega > \omega$, as we have observed.

IV. CONCLUSION AND DISCUSSIONS

In conclusion, we have generalized the usual vibrational resonance in bistable systems subject to a biharmonic force with very different frequencies to any two frequencies, and found that the system response to the weak signal can be optimized by the other signal with an intermediate amplitude and an appropriate frequency. When the frequency is exactly a multiple of the low frequency, the resonance can even get stronger, signaling the occurrence of a frequency-resonance-enhanced vibrational resonance. Clearly this is a unique type of resonance. It is fundamentally different from a pure vibrational resonance or frequency resonance, but nevertheless it combines the mutual action of vibrational resonance, which is an essential dynamical bifurcation effect, and frequency resonance as well, which is an essential frequency match effect. Therefore, it is quite natural that it should depend on the values of both the amplitude and frequency. These behaviors are universal, as several other frequency parameters (e.g., $\omega = 0.05$ or 0.1) have been systematically tested and all qualitative results have been found unchanged.

Below it is necessary to give some further discussions. It is well known that both the stochastic resonance with a white noise and vibration resonance, where a high-frequency signal plays the role of a white noise, can be considered in a unique framework [37]. It is interesting to compare the results of the present work with the results of stochastic resonance generated by an exponentially correlated noise, where the noise correlation time might play the role of a period of a strong harmonic signal [38]. The system dynamics is given by

$$\begin{aligned} \dot{x} &= x - x^3 + A\cos(\omega t) + y(t), \\ \dot{y} &= -\tfrac{y}{\tau} + \frac{\sqrt{2D}}{\tau}\xi(t), \end{aligned} \tag{8}$$

where $\xi(t)$ is a Gaussian white noise with correlation $\langle \xi(t)\xi(s)\rangle = \delta(t-s)$ and D denotes the noise strength. This colored noise $y(t)$ therefore possesses the following correlation:

$$\langle (t)y(s)\rangle = \frac{D}{\tau}\exp^{-|t-s|/\tau}, \tag{9}$$

with τ being the noise correlation time. Clearly the colored noise $y(t)$ approaches the case of white noise as $\tau \to 0$. In the numerical simulations of Eq. (8), the standard Heun scheme is used, and the same system parameters $A = 0.1$ and $\omega = 0.2$ are chosen. The result for the system response Q as a function of $2\pi/\tau$ and D is shown in Fig. 8(a). For the x axis, τ is changed linearly from $\tau = 0.01$ to 2 with $\Delta\tau = 0.01$. In Fig. 8(b), the dependence of Q on D for two different τ's, $\tau = 0.01$ and 2.0, is displayed. From these plots, we can clearly see that Q nonmonotonically depends on the value of noise strength D, indicating the occurrence of the usual stochastic resonance. Under this situation, the high-frequency signal in Eq. (1) in vibrational resonance *does* play a similar role of noise. However, we *do not* find a significant resonance curve (Ω^*, B^*) and a frequency-resonance-enhanced vibrational resonance

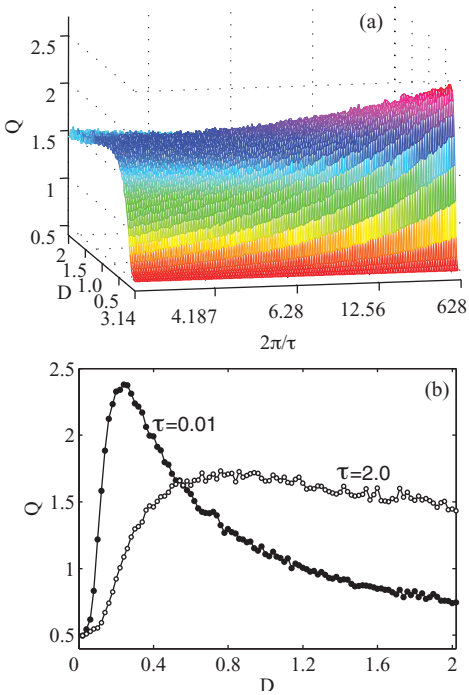

FIG. 8. (Color online) (a) The 3D plot of response Q as a function of $2\pi/\tau$ and D for the noisy system (8). In the x axis, the value of τ is linearly scanned from $\tau = 0.01$ to 2.0, with $\Delta\tau = 0.01$. The parameters $A = 0.1$ and $\omega = 0.2$ are fixed and the same as in Fig. 1, to be compared with system (1). (b) Q vs D for $\tau = 0.01$ and 2.

peaks for the noisy system (8), after comparing these two corresponding 3D plots. Intuitively, the noise correlation time is still not a pure time scale, which certainly cannot produce a strong time-scale match (or frequency match) effect as we have seen in the frequency-resonance-enhanced vibrational resonance.

Finally, it is worth noting that two-frequency signals with very different frequencies (as in the case of the vibration resonance) are important for communication, since a low-frequency signal modulates a high-frequency carrier signal, and is also an object of interest in several other important fields. For the case considered in the present paper, the condition for two sufficiently different frequencies is unnecessary and some possible applications are still obvious and wide. Examples include a technique for the display of picosecond laser pulses using two different optical frequencies [39], the pitch perception of two-frequency stimuli by the human ear in acoustics [40], the Faraday waves in a pattern formation with two-frequency parametric excitation (one is the signal frequency ω and the other is the subharmonic frequency $\omega/2$) [41], neurobiological reaction controlling by electrical stimulation of different frequencies [42], and so on. Therefore, we believe that all these findings are of not only interest for researchers in nonlinear dynamics, but also valuable in engineering for potential applications.

ACKNOWLEDGMENTS

This work was partially supported by the Bairen Jihua Foundation of Chinese Academy of Sciences and the National Natural Science Foundation of China under Grant No. 11075202. We thank the two reviewers very much for their comments and suggestions.

[1] K. Wiesenfeld and F. Moss, Nature (London) **373**, 33 (1995).
[2] P. Jung and P. Hänggi, Phys. Rev. A **44**, 8032 (1991).
[3] L. Gammaitoni, P. Hänggi, P. Jung, and F. Marchesoni, Rev. Mod. Phys. **70**, 223 (1998).
[4] Hu Gang, H. Haken, and C. Z. Ning, Phys. Rev. E **47**, 2321 (1993).
[5] L. Gammaitoni, F. Marchesoni, E. Menichella Saetta, and S. Santucci, Phys. Rev. Lett. **62**, 349 (1989).
[6] J. M. G. Vilar and J. M. Rubi, Phys. Rev. Lett. **77**, 2863 (1996).
[7] P. Jung and G. Mayer-Kress, Phys. Rev. Lett. **74**, 2130 (1995).
[8] P. C. Gailey, A. Neiman, J. J. Collins, and F. Moss, Phys. Rev. Lett. **79**, 4701 (1997).
[9] D. Cubero, Phys. Rev. E **77**, 021112 (2008).
[10] B. McNamara and K. Wiesenfeld, Phys. Rev. A **39**, 4854 (1989).
[11] B. McNamara, K. Wiesenfeld, and R. Roy, Phys. Rev. Lett. **60**, 2626 (1988).
[12] P. S. Landa and P. V. E. McClintock, J. Phys. A **33**, L433 (2000).
[13] I. I. Blekhman and P. S. Landa, Int. J. Nonlinear Mech. **39**, 421 (2004).
[14] M. Gitterman, J. Phys. A **34**, L355 (2001).
[15] I. I. Blekhman, *Vibrational Mechanics. Nonlinear Dynamic Effects, General Approach, Applications* (World Scientific, Singapore, 2000).
[16] A. Maksimov, Ultrasonics **35**, 79 (1997).
[17] J. D. Victor and M. M. Conte, Visual Neurosci. **17**, 959 (2000).
[18] D. Su, M. Chiu, and C. Chen, Precis. Eng. **18**, 161 (1996).
[19] V. Gherm, N. Zernov, B. Lundborg, and A. Vastberg, J. Atmos. Sol.-Terr. Phys. **59**, 1831 (1997).
[20] E. D. Kaplan, *Understanding GPS: Principles and Applications* (Artech House, London, 1996).
[21] E. Ullner, A. Zaikin, J. García-Ojalvo, R. Bascones, and J. Kurths, Phy. Lett. A **312**, 348 (2003).
[22] C. Stan, C. P. Cristescu, D. Alexandroaei, and M. Agop, Chaos, Solitons Fractals **41**, 727 (2009).
[23] D. Cubero, J. P. Baltanás, and J. Casado Pascual, Phys. Rev. E **73**, 061102 (2006).
[24] B. Deng, J. Wang, and X. L. Wei, Chaos **19**, 013117 (2009).
[25] J. Casado Pascual and J. P. Baltanás, Phys. Rev. E **69**, 046108 (2004).
[26] V. N. Chizhevsky and G. Giacomelli, Phys. Rev. E **73**, 022103 (2006).
[27] V. N. Chizhevsky and G. Giacomelli, Phys. Rev. E **70**, 062101 (2004).
[28] V. N. Chizhevsky and G. Giacomelli, Phys. Rev. A **71**, 011801 (2005).
[29] A. A. Zaikin, L. López, J. P. Baltanás, J. Kurths, and M. A. F. Sanjuán, Phys. Rev. E **66**, 011106 (2002).
[30] V. M. Gandhimathi, S. Rajasekar, and J. Kurths, Phys. Lett. A **360**, 279 (2006).
[31] C. G. Yao and M. Zhan, Phys. Rev. E **81**, 061129 (2010).
[32] V. N. Chizhevsky, E. Smeu, and G. Giacomelli, Phys. Rev. Lett. **91**, 220602 (2003).
[33] J. P. Baltanás, L. López, I. I. Blechman, P. S. Landa, A. Zaikin, J. Kurths, and M. A. F. Sanjuán, Phys. Rev. E **67**, 066119 (2003).
[34] R. P. Feynman, *The Feynman Lectures on Physics* (Addison-Wesley, Boston, MA, 1964).
[35] Z. L. Qu, G. Hu, G. Yang, and G. R. Qin, Phys. Rev. Lett. **74**, 1736 (1995).
[36] S. T. Vohra, L. Fabiny, and K. Wiesenfeld, Phys. Rev. Lett. **72**, 1333 (1994).
[37] P. S. Landa, I. A. Khovanov, and P. V. E. McClintock, Phys. Rev. E **77**, 011111 (2008).
[38] P. Hanggi, M. E. Inchiosa, D. Fogliatti, and A. R. Bulsara, Phys. Rev. E **62**, 6155 (2000).
[39] P. M. Rentzepis and M. A. Duguay, Appl. Phys. Lett. **11**, 218 (1967).
[40] G. F. Smoorenburg, J. Acoust. Soc. Am. **48**, 924 (1970).
[41] M. Silber and A. C. Skeldon, Phys. Rev. E **59**, 5446 (1999).
[42] J. S. Han, Trends Neurosci. **26**, 17 (2003).